CIRP Journal of Manufacturing Science and Technology 51 (2024) 36–46

Contents lists available at ScienceDirect

CIRP Journal of Manufacturing Science and Technology

journal homepage: www.elsevier.com/locate/cirpj

# Frictional behaviour of coated carbide tools and AISI 316L when using translational and rotatory relative movement considering dry and lubricated conditions

Pascal Volke [a,*], Cédric Courbon [b], Erik Krumme [a], Jannis Saelzer [a], Joel Rech [b], Dirk Biermann [a]

[a] Institute of Machining Technology (ISF), Technical University Dortmund, Baroper Straße 303, 44227 Dortmund, Germany
[b] University of Lyon, Ecole Centrale de Lyon – ENISE, LTDS, UMR CNRS 5513, 58 Rue Jean Parot, 42100 Saint-Etienne, France

ARTICLE INFO

*Keywords:*
Tribology
Friction
Coating
Lubrication
Orthogonal cutting
Finite element modelling

ABSTRACT

In machining, tool temperatures and thus tool wear are significantly influenced by frictional behaviour. Friction tests are used to determine the friction coefficient depending on relative speed, which serves as basis for parameterising friction models as input data for chip formation simulations. Therefore, this paper represents investigations towards the frictional behaviour of uncoated and coated (TiN, TiAlN) carbide tools when using two different relative movements (translational and rotary) and cooling lubricant conditions. In dry conditions, the investigations show insignificant influence of different engagement surfaces and testing kinematics on resulting friction. In lubricated conditions, three different friction coefficient sections were observed.

## 1. Introduction

Friction and wear occur in almost all technical applications and therefore play an important role in the improvement of engineering systems. In this context, the chip formation zone represents a particularly challenging case due to the high contact normal stresses, temperatures, and relative speeds as well as the wide range of tribo-partners (tool and workpiece) and intermediate media (cooling lubricants) used [1]. Even though approaches exist to characterise the frictional behaviour directly from cutting investigations [2], this complex tribological system is still only accessible to a limited extent in these tests. Therefore, various equivalent test rigs have been developed for fundamental friction characterisation under so-called machining-like conditions [3]. In addition to the understanding thus generated, the data often serve as the basis for parameterising empirical friction models in chip formation simulations [4]. Initially, general familiar approaches such as the pin-on-disk test were taken and adapted to cutting machine tools [5]. However, these have the disadvantage that they are closed tribometers. This does not correspond to the processes in the chip formation zone, which is an open tribological system [3]. Sterle et al. could prove within a comparative study that an open tribometer results in significantly higher coefficients of friction than a closed one [6]. In order to bring the tribometer closer to the conditions in the chip formation zone, a few different open tribometer have been developed. Here, among other things, a distinction can be made between test principles with rotating relative motion and those with translational relative motion.

As far as rotary tribometers are concerned, a popular configuration (Figs. 1**a, b, c** ) uses a pin placed just after a cutting tool during the machining of a tube face [7–9]. In this case, the pin rubs against a continuously refreshed surface and the relative speeds and contact temperatures replicate dry or lubricated machining.

The experimental set-up in Fig. 1**d** is similar to orthogonal cutting on a disc using a real cutting tool with an extremely negative rake angle [10]. However, during a single rotation of the workpiece and really short friction time, it is difficult to achieve a steady thermal state.

As an alternative, an open tribometer simulating the contact conditions in cutting over a longer time scale (Figs. 1**e, f** ) was proposed [11]. A cylindrical pin rubs on a fresh surface during rotation and the surface refreshment is discontinuous. A large feed of the pin enables a helical movement in order to avoid superposition of the scratches produced on the cylinder. This tribo-set-up, installed on a lathe, can yield sufficiently high relative speeds (several hundred m/min).

The latest tribometer (Fig. 1e) has been involved in several investigations dealing with the influence of a cooling lubricant. It was improved by Mondelin et al. to reach higher contact pressures and relative speeds. In addition, it also provides, through special

* Corresponding author.
*E-mail address:* pascal.volke@tu-dortmund.de (P. Volke).

https://doi.org/10.1016/j.cirpj.2024.03.011
Received 16 October 2023; Received in revised form 21 March 2024; Accepted 31 March 2024
Available online 12 April 2024

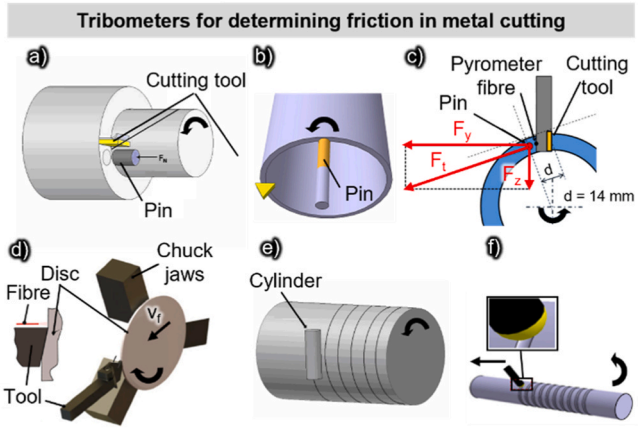


**Fig. 1.** Tribometers for determining friction in cutting with rotatory relative movement. Designed by (a) Olsson et al. [7], (b) Zemzemi et al. [9], (c) Smolenicki et al. [8], (d) Puls et al. [10]. (e) Hedenquist et al. [11], (f) Mondelin et al. [12].

instrumentation, the heat partition at the interface, which is a key thermal parameter in numerical simulations [12]. In Fig. 2 it can be seen that the use of a lubricant oil causes a large decrease in the friction coefficient, especially at low relative speeds.

In contrast, the effect is less at higher relative speeds relative to the dry case. In the presence of a mineral or a vegetable oil, the friction coefficient remains constant around 0.1 irrespective of the relative speed. On the contrary, an emulsion leads to almost twice higher friction coefficients regardless of the relative speed.

Other investigations [12] and [13] have revealed that friction behaviour strongly depends on the amount of cutting fluid supplied, its viscosity, and the contact duration. It was shown that oil was eliminated in a few tenths of a second due the high contact pressure and relative speed. On the other hand, oil will penetrate the tool-chip interface if the contact is longer than a second (turning, drilling, etc.). In interrupted cutting processes, the contact is lubricated before each cutting period. The amount of oil deposited at the interface (before cutting) depends strongly on the cutting speed. At high cutting speeds, oil starvation leads to dry sliding [12].

The principle of Puls et al. (see Fig. 1d) was transferred to a translational relative motion. Within the following investigations different factors have been varied e.g., relative speed, temperature, and workpiece material. It turned out that especially for contact between

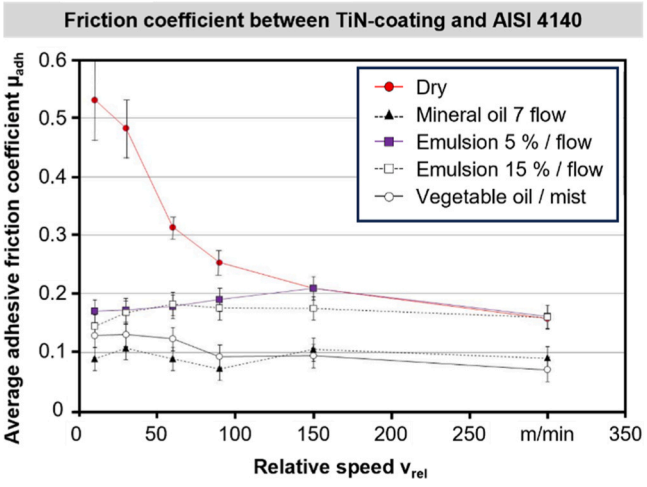


**Fig. 2.** Influence of various cutting fluids on adhesive friction coefficient between TiN coated tool and AISI 4140 steel, based on [12].

cemented carbide and steel (AISI 4140) the relative speed has a significant influence on the resulting friction coefficient. With increasing relative speed, the friction coefficient decreases [14]. Using the same experimental principle, Saelzer et al. investigated the influence of different surface topographies on uncoated cemented carbide bodies in contact with AISI 1045 steel. While a polished and a microfinished surface, which both have only very small roughness peaks showed a similar course over the relative speed, a wet abrasive blasted surface led to significantly lower friction coefficients for relative speeds between $v_{rel} \approx 30$ m/min and $v_{rel} \approx 100$ m/min. The authors attributed this correlation to the comparatively smaller real contact area at the dimple structure. For higher relative speeds the surface topography takes a back-seat and further increasing relative speed from $v_{rel} = 150$ m/min on only leads to a small change of friction coefficients [16]. Within a following study, Saelzer et al. added a high-viscosity oil as intermediate medium to the experiment. The coefficients of friction were significantly reduced compared to dry contact, especially for low relative speeds and could less be influenced by surface topography [17].

Concerning the influence of tool coatings, the picture is more unclear. In some cases influences on friction could be identified for others not [18,19]. Nobel et al. conducted experiments with the experimental setup from Puls et al. on brass alloys. While a titanium diboride coating led to nearly no changes in the frictional loads compared to an uncoated tool, a diamond-like carbon coating significantly reduced them for two of the four investigated materials. The authors claim that this influence is caused by the different hardness, lattice structure, chemical affinity as well as the surface topography of the coating [15]. Many possible causes are known for the influence of the coatings, but it is often not possible or has not been carried out to consider them separately. In particular with regard to the coating and the surface topography, the influences are often presented as superimposed, although differentiation is possible here by means of a targeted coating post-treatment. In addition, the question arises as to the influence of the used tribometer [20]. The same applies to lubrication effects from intermediate media used. In principle, the literature shows that significant reductions in frictional loads can be observed in the course of equivalence tests under machining-like conditions [13,17,21]. However, the intensity of this reduction in force or reduction in the friction coefficient varies greatly from study to study. The superimposed influences of the type of lubricant, the material pairing, the test principle as well as possible coatings and surface topographies are far from being fully understood [22]. In the course of investigations into the influence of lubricants, tribo-chemical mechanisms in particular are often not taken into account. Although detailed experiments have already been carried out on these interrelationships [23,24], understanding is still limited and knowledge about them is not widespread among machining experts.

Only a few publications could be used as a direct reference for the material pairing investigated in this study, as the stainless steel AISI 316L was only examined in a few publications with regard to its frictional properties under machining-like conditions. Valiorgue et al. investigated the contact between AISI 316 L and TiN-coated cemented carbide using a pin-on-bar test. At a relative speed of $v_{rel} = 60$ m/min and a normal force of $F_n = 400$ N, they determined friction coefficient of $\mu = 0.8$ and a relative speed-related decrease to $\mu = 0.53$ at $v_{rel} = 180$ m/min. For an increased normal force ($F_n = 1000$ N), friction coefficients of $\mu = 0.72$ for $v_{rel} = 60$ m/min and $\mu = 0.38$ for $v_{rel} = 180$ m/min resulted [25]. Bonnet et al. determined under similar test conditions for a normal force of $F_n = 1000$ N, corresponding to an average normal contact pressure of $p_n = 1.8$ GPa, an apparent friction coefficient of $\mu \approx 0.4$ at $v_{rel} = 60$ m/min. Increasing the relative speed to $v_{rel} = 180$ m/min led to a decrease in friction coefficient to $\mu \approx 0.25$ [26]. In view of the fact that the values available in the literature show a certain degree of deviation, further investigation is highly relevant.

This is where the present study comes in, using two equivalent test rigs to investigate friction and lubrication in contact of the challenging stainless steel material AISI 316L with uncoated and TiN-coated

cemented carbide. One experimental setup involves a translational relative motion with a trapezoidal contact surface using the actual cutting tools. In the second experimental setup, a rotational relative motion takes place in a pin-on-cylinder test. In both experimental setups, tests were performed varying the relative speed both in dry conditions and using an oil-based cooling lubricant. Using the translational test setup, further investigations were carried out on the influence of the tool coating (TiN and TiAlN) with constant type of surface topography on the frictional load. The experimental boundary conditions as well as the results and analyses of the tests are presented in the following. The paper concludes by showing how the experimental results can be used to parameterise empirical models of the friction coefficient for numerical chip formation simulations.

## 2. Experimental boundary conditions

### 2.1. Experimental equipment

As part of the investigations, friction characterisations of different counter body (CB) and main body (MB) pairing were carried out on two different machine tools with unequal kinematics. The comparative research focus was to investigate the frictional behaviour by an evaluation of the friction coefficients, contact pressures and temperatures under varying the relative speed, lubrication condition, contact conditions and normal loads as well as the coating. The variables and evaluated parameters, that are depending on the experimental setup, are illustrated in the experimental plan in Table 1.

Two different machine tools are used, equipped with various test rigs. On the one hand, a special machine tool in gantry design from *BERGER Group* with translational kinematics comes into operation. Owing to a linear drive (x-axis) it is capable to achieve a relative speed of $v_{rel} = 180$ m/min at a maximum movement of $l = 900$ mm, see Fig. 3.

On the other hand, a lathe TC25 Y by *CMZ Machinery Group*, which is equipped by a special constructed tribometer, is used. This machine has a rotary kinematics, whereby the maximum spindle speed of 4000 rpm, the operating diameter of 140 mm (x-axis) and length of 500 mm (z-axis), constrained by the experimental setup, being the restriction for the maximum relative speed and friction path.

### 2.2. Work and tool materials

#### 2.2.1. Translational relative movement

For both tests rigs, the CB was made of steel AISI 316L. The austenitic steel has a yield stress of $R_{p0.2} = 277$ MPa and an average hardness of 215 HV10. The initial diameter of the forged and peeled workpiece was $d = 165$ mm. For translational movement, the sample preparation was done by an eroding process. Thus, a sample with the dimensions $b = 2$ mm, $h = 50$ mm and $l = 140$ mm was produced. As MB, uncoated and coated cemented carbide (fine-grained) cutting tools type TPU-N160304EN were used. For coating, monolayer TiN and TiAlN with an averaged coating thickness of $t_{TiN} = 3.7$ µm and $t_{TiAlN} = 5.2$ µm were applied, deposited with cathodic arc physical vapour deposition (PVD). The surface topography including the arc cathodic typical droplets,

**Table 1**
Experimental plan and investigated parameters.

| | | Translational | Rotatory |
|---|---|---|---|
| Variables | $v_{rel}$ | 10 … 180 m/min | 10 … 300 m/min |
| | Infeed, a | 0.1 mm | $a(F_n)$ |
| | Coating | Uncoated, TiN, TiAlN | TiN |
| | Lubrication | Dry/Blaser Vascomill MMS HD1 | Dry/Blaser Vascomill MMS HD1 |
| | Used jack | - | Pneumatic/Hydraulic |
| Target measurement variables | | Friction coefficient, µ<br>$p_{app}$ (experimental)<br>Temperature, T | Friction coefficient, µ<br>$p_{app}$ (simulative)<br>- |

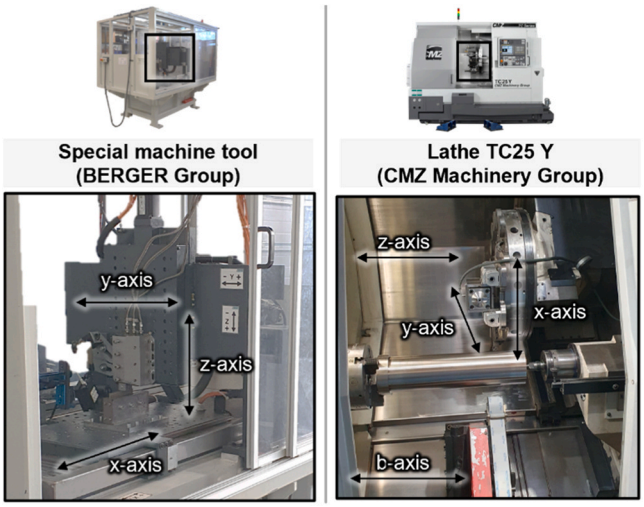


**Fig. 3.** Comparison of the machine tools used: special machine with translatory movement vs. lathe with rotary movement.

which are smoothed by the normal forces acting in the process, as well as the cutting edge radius of the tools are shown in Fig. 4. Since the surface roughness is comparable for all tool variants, a more isolated comparison of the friction characteristics, independent from surface roughness, can be elaborated. The cutting edge radius was set to $r_\beta \approx 40$ µm, thus achieving improved coating adhesion and reducing the risk of initial cutting edge chipping. The latter is of central importance for analysing the wear evolution of the tools, which is planned in the further course of the project.

#### 2.2.2. Rotatory relative movement

For the CB, a cylindrical bar with a diameter of $d = 140$ mm and a length of $l = 500$ mm was used. As MB, pins made of cemented carbide with a similar grade to the one used for cutting tools dedicated for machining AISI 316L were used (see Fig. 5).

The diameter was $d = 8$ mm, and the radius of the spherical segment cap was $r_{Sphere} = 8.5$ mm. They were coated with TiN coating deposited by PVD (cathodic arc 2 µm monolayer). A TiAlN coating was not applied, as the comparison of the tribometers is restricted to the TiN-coating. In order to eliminate the potential influence of surface roughness, the pins were polished after the coating process to reach a low surface roughness Ra = 0.1 µm), which is similar to a typical surface roughness on a finely ground carbide cutting tool. Concerning bars, after each friction test, a cutting tool refreshes the surface ploughed by the

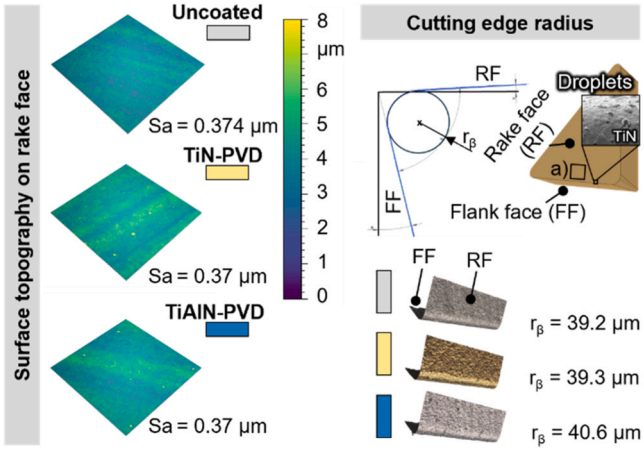


**Fig. 4.** Experimental tools: Rake face of the tool (main body), serves as friction surface.

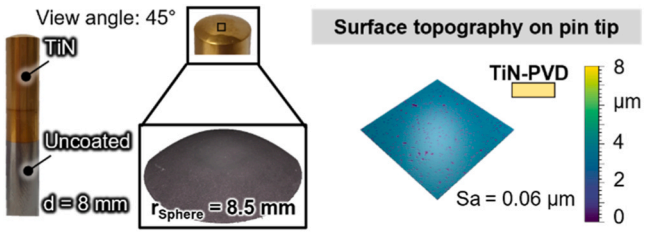


**Fig. 5.** Dimensions and surface Roughness of TiN-coated Pins.

pin. A belt finishing operation was also performed in order to obtain a very low surface roughness Ra = 0.1 µm) and a constant surface for each test.

### 2.3. Experimental setup

#### 2.3.1. Translational relative movement

The investigations with translational relative motion were conducted on a test rig based on Puls et al. [10]. For implementation, the x-axis of the special machine tool was responsible for realising the required relative speed $v_{rel}$. The vertical portal, consisting of two axes, was used for setting the infeed $a_r$ (y-axis) and positioning the MB (z-axis), see Fig. 3. Fig. 6 illustrates that the CB was fixed on the machine table.

On the vertical portal, a three-component dynamometer from *Kistler group* type 9263, that clamps a specially designed MB/tool holder, was installed. The sampling rate was set to f = 1000 Hz, whereby the average acquisition time depends on the relative speed set. The MB was fixed at an inclination angle of $\lambda_r = 5°$ in the tool holder. A magnet secures the MB inside the insert seat allowing the rake face of the tool acts as friction surface. The translational relative motion imprinted on the table as well as the infeed $a_r$ puts the MB and CB into contact. Considering the angle of inclination $\lambda_r$, the measured process forces can be used to determine a friction force $F_r$ and a normal force $F_n$, whose quotient describes the friction coefficient μ based on Coulomb's friction model. To determine the temperature on the CB a two-colour pyrometer was used. Here, the fibre optic was placed with a distance of l = 0.8 mm behind the MB. The measurements were carried out at relative speeds of $v_{rel}$ = 29; 89; and 180 m/min for each coating. As lubrication, Vascomill MMS HD 1 from *Blaser* was used. The ester-based oil (80% Ester) has a viscosity of v = 40 $mm^2/s$ at 40 °C, with a sulphur content of 16% and a density of ρ = 1.00 $g/cm^3$ . The oil was directly applied onto the MB before the test started, whereby the maximum quantity was given by the limited surface tension of the oil.

#### 2.3.2. Rotatory relative movement

The tribometer used has been developed and further enhanced by Mondelin et al. [12]. A cylindrical pin rubs on a fresh surface during rotation. A large feed of the pin enables a helical movement in order to avoid superposition of the scratches produced on the cylinder. This tribo-set-up, installed on a lathe, can yield sufficiently high relative speeds (several hundred m/min) and high forces (high stiffness), see Fig. 7.

To adapt a constant normal force to the pin, a pneumatic jack from *FIBRO* type 2482.74 was used with a maximal applicable normal force of $F_N$ = 300 N. This represents Option A, where the normal force is set by the penetration depth. Due to adhesive material behaviour and the resulting induced vibrations, a hydraulic jack was used with a maximum applicable pressure of p = 100 bar (equals an approx. normal force of $F_n$ = 1000 N) as option B. Here, the normal force is set by the selected pressure. The main difference between both jacks is the induced stiffness and the resulting displaced natural frequency of the system, what is based on different active mediums. As the oil of the hydraulic jack is less compressible, it leads to a greater stiffness of the tribometer.

Each friction test lasts approximately t = 10 s. The pin holder was fixed onto a dynamometer from *Kistler group* type 9367C with a sampling rate of f = 1000 Hz in order to provide the normal force $F_N$ and tangential force $F_t$ (macroscopic forces). The apparent friction coefficient is also provided by the ratio between the tangential and the normal forces, taken as an average value of the stationary zone. The term apparent friction coefficient is used because it differs significantly from the interfacial friction coefficient. In this work, it is assumed that adhesion is the main mechanism of friction at the pin–work material interface. Indeed, the macroscopic forces measured by the tribometer include the friction phenomena (adhesion) and the plastic deformation of the work material. For lubricated tests, the same oil was used as in the translational test rig. The oil application was different compared to translational test rig because it was applied directly onto the CB.

## 3. Experimental results

In the following chapter, the results of the experimental investigations are described and analysed. First, the experiments with translational relative motion are presented. Subsequently, the results of the tests with rotating relative motion are shown, followed by a general discussion of the experimental results based on a comparison of the two test rigs.

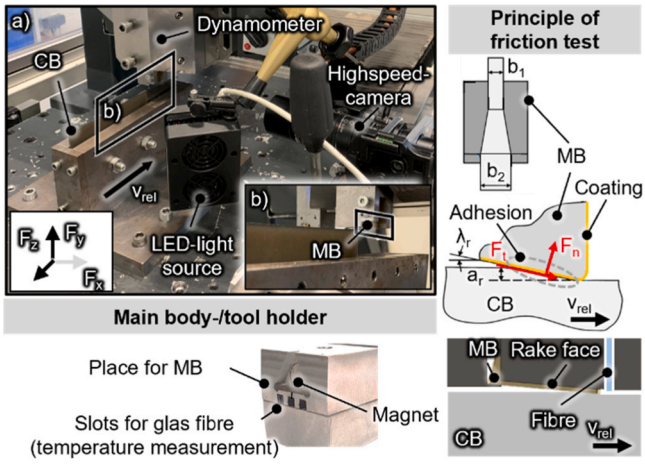


**Fig. 6.** Experimental setup: Friction characterisation by translational relative movement.

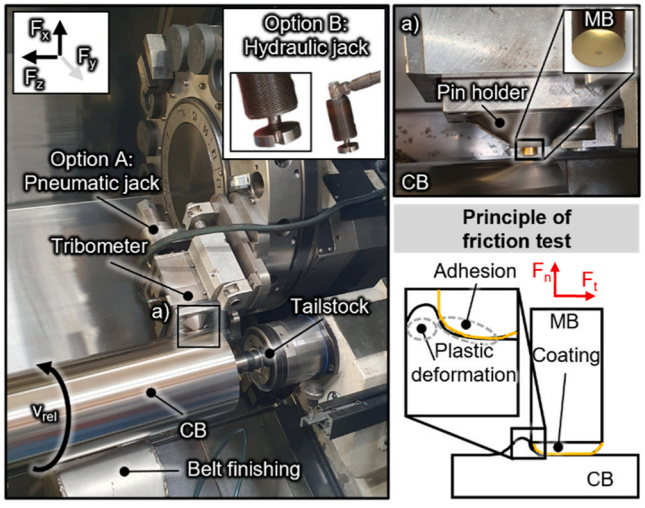


**Fig. 7.** Experimental setup: Friction characterisation by rotatory relative movement.

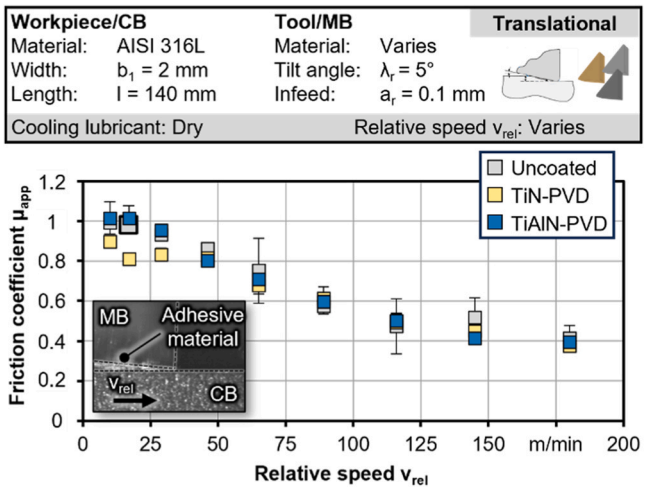


**Fig. 8.** Friction coefficients depending on the relative speed and coating.

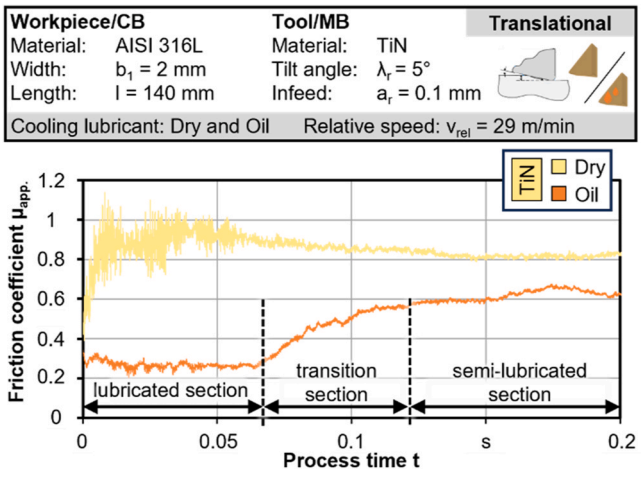


**Fig. 9.** Friction coefficients in relation to process time for different cooling lubrication strategies.

### 3.1. *Translational relative movement*

Fig. 8 shows the coefficients of friction as a function of relative speed for different tool coatings. In general, the trend known from the literature can be seen that the coefficients of friction are relatively constant at high values at low relative speeds ($v_{rel} < 40$ m/min), decrease with further increase of the relative speed and finally approach a limit value from approx. $v_{rel} = 100$ m/min.

This behaviour can be explained by the fact that at very low relative speeds, due to the comparatively low temperatures, the contact situation is characterised by significant material build-up, which entails high coefficients of friction (see Fig. 8). This behaviour is comparable with built-up edge formation and, in the case of austenitic steel tending to adhesion, leads to coefficients of friction of $\mu \approx 1$, which, by definition, is in the limit of friction and tends to be accompanied by adhesion with internal sliding of the material. In their friction tests, Mondelin et al. were able to make similar observations, see Fig. 2 [12]. The lower level of the friction coefficient can be explained by calculating the adhesive friction coefficient, meaning that the plastic deformation based friction component, still has to be added. The significant difference in the friction coefficient at relative speeds of $v_{rel} < 100$ m/min can be explained by the material used, as it has a significantly lower tendency to adhesion compared to AISI 316 L.

The subsequent decrease in the friction coefficient with increasing relative speed can be explained by the fact that the tendency to adhesion decreases due to higher temperatures and shorter contact times, and mechanical friction mechanisms operate under lower resistance due to the increasing temperature. As already described in other references [14,16], it is assumed that from a relative speed of $v_{rel} = 100$ m/min, a thin, nearly molten intermediate layer forms between the tribological partners, which limits the influence of a further increase in relative speed on the friction coefficient. Experimental proof of the partially liquefied layer cannot be obtained.

The influence of the coatings on friction, which in this case could be investigated almost independently of the influence of the surface roughness, turns out to be relatively low overall. Only in the range of low relative speeds ($v_{rel} < 40$ m/min) do systematically lower friction coefficients occur in the contact of the steel material with the TiN-coated surface than for the uncoated and the TiAlN-coated MB. This can be explained by a slightly lower tendency to adhesion formation of this coating.

In addition to the influence of the coatings, the influence of an intermediate medium was investigated. The tool was kept constant, and all tests were carried out with the TiN coating determined to be slightly advantageous. Fig. 9 shows two parallelised measurement records of the friction coefficient over the test period for a dry and a lubricated test. In the case of the dry test, after a steep increase at the beginning of the measurement, there is a range of initial friction characterised by larger fluctuations.

It is possible that a stick-slip effect occurs here due to constantly changing temperature conditions. As the measurement progresses, the friction coefficient becomes increasingly stationary. The course of the lubricated test differs significantly from the dry one. At the beginning of the measurement, the friction coefficient is only about one third of the mean value for the dry case. In addition, the curve exhibits no pronounced fluctuations. After a certain test period, a transitional range is then established in which the friction coefficient increases continuously. Finally, it then transitions to an approximately stationary course. Although this is at a more than doubled level compared to the beginning of the measurement, it is still significantly below the curve of the dry test. It is assumed that a lubricating film is established at the beginning, which is essentially characterised by hydrodynamic liquid lubrication. Due to the high mechanical and thermal loads and the kinetic resistance of the chip movement, this is a lubrication condition that can only be found in the chip formation zone at low cutting speeds [27]. In the friction tests, however, this can be regulated across all tests. This is mainly due to the fact that the cooling lubricant is drawn into the lubrication gap in the test configuration, whereas in the chip formation zone it has to penetrate the lubrication gap against the chip movement. Above a certain temperature level, this lubricating film is then gradually degraded over the transition section within the contact surface until it is finally completely dissolved. The service life of the lubricating film decreases with increasing relative speed, as critical temperatures are reached in a shorter time with higher friction power. There are two possible explanations for the remaining lubrication in the semi-lubricated part. On one hand, residues of the intermediate medium could have remained in closed cavities of the contact zone and provide hydrostatic lubrication there. On the other hand, reaction-products of the iron from steel material and the sulphur from the cooling lubricant, which are known to have a lubricating character [23,24] could have been formed in the contact zone. The two literature sources mentioned above attribute this to the formation of iron sulphide and iron

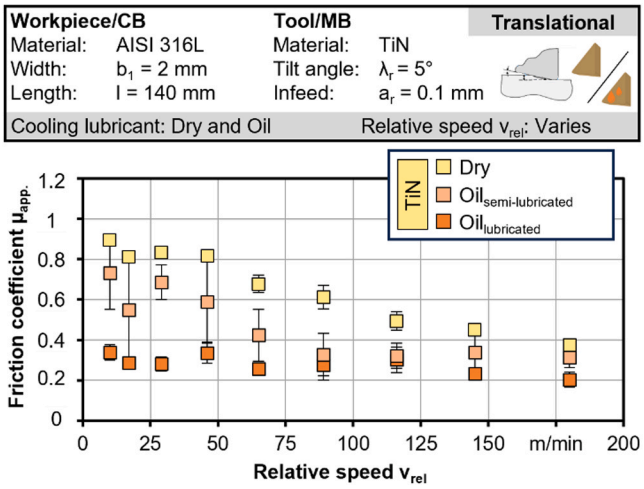


**Fig. 10.** Friction coefficients depending on the relative speed considering different cooling lubrication concepts.

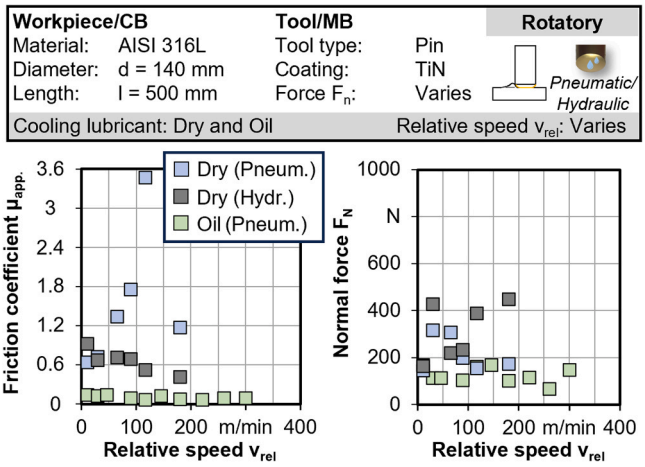


**Fig. 11.** Influence of the relative speed on the critical normal force and the friction coefficient.

disulphide, which they detected using energy-dispersive X-ray spectroscopy (EDX), X-ray photoelectron spectroscopy (XPS), auger electron spectroscopy (AES) and transmission electron microscopy (TEM). This study did not have all the analytical options available to provide reliable evidence of this. This will be the subject of future studies. Overall, therefore, it is evident that a significant influence on the frictional loads could be caused by an intermediate medium and that different sections of lubrication occurred in the process.

Fig. 10 shows the results of all the individual measurements, as exemplified in Fig. 9, in a plot of the friction coefficient versus relative speed.

Three different conditions are distinguished dry, lubricated, and semi-lubricated. Mean values of the friction coefficient were calculated in the respective stationary range of the curves, while the values for the dry tests were taken from Fig. 8. It can be seen that the lubricated state over the entire series of tests is at a significantly lower level than the dry case, whereby the dependence on the relative speed is significantly lower than for the dry case. This results in an increasing convergence of the curves for an increasing relative speed. The values for the semi-lubricated state lie between the other two for all tests, although for low relative speed a greater closeness to the dry course can be observed, both qualitatively and quantitatively. From speeds of more than $v_{rel}$ = 40 m/min, the curve then drops significantly faster than the dry one and clearly approaches the value of the lubricated state in the range of $v_{rel}$ = 90 m/min. Like the other courses, no further significant change in the friction coefficient occurs with a further increase in relative speed. Based on this behaviour, it can be assumed that the semi-lubrication is primarily due to tribo-chemical reaction products, since the effect is less pronounced at low relative speeds, where lower temperatures occur than at high relative speeds. Since the chemical reactions are, among other things, temperature-driven and remaining oil in cavities would tend to lose effect as temperatures increase this conjecture can be concluded.

### 3.2. Rotatory relative movement

Fig. 11 shows the influence of the relative speed as well as the lubrication on the friction coefficient and normal force $F_N$. The testing series were conducted using two different set-ups of the tribometer, as described above. The friction coefficient is on a significantly lower level in lubricated conditions than under dry ones. This can be explained by the lubricating film, which is responsible for hydrodynamic lubrication. Thus, the intermediate medium (oil) ensures a significant reduction of adhesive-related mechanical clamping between the MB and the CB, especially for small relative speeds. For increasing relative speeds up to $v_{rel}$ = 116 m/min, the friction coefficient slightly decreases. This can be explained through the decrease of tangential forces, though higher prevailing temperatures. Nevertheless, a slightly increase of the friction coefficient for relative speeds greater than $v_{rel}$ > 116 m/min can be observed. This can be attributed to the discontinuous supply of the oil only before the start of the test. The capillary force of the oil which holds the oil on the bar could be exceeded by the centrifugal forces which occur through the rotation of the bar. As a result, a decrease of thickness of the lubrication film arises and leads to a slightly increase of friction coefficient, see Fig. 11.

While using the pneumatic jack under dry conditions, no course comparable with the literature could be determined, as it can be seen in Fig. 11. For a relative speed of less than $v_{rel}$ < 89 m/min, the coefficient of friction remains at a comparable level. At relative speeds greater than $v_{rel}$ > 89 m/min, stick-slip motion occurs, which causes oscillating loads, including an overloading of the jack. The friction and thus the measured coefficient of friction becomes unstable, reaching its maximum at a relative speed of $v_{rel}$ = 116 m/min with a coefficient of friction of μ = 3.6. This contradicts the confirmed assumption that the friction coefficient decreases with increasing relative speeds. The deviation in the dry condition testing series can be explained by the mentioned stick-slip effects, which occur due to the adhesive material behaviour. Through stick-slip related effects and a material built-up in front of the pin (plastic deformation), the maximum applicable normal force of the pneumatic jack is exceeded. The pneumatic jack is elastically compressed as a result of the high normal forces, which leads to an actuation of the system with natural oscillations. The high coefficients of friction can then be associated with minimum normal loads during the load oscillation cycle, while the friction force remains high. Hence, the stiffness of the system is not sufficient for adhesive material behaviour, which occur during the dry condition testing series.

To raise the limit of the maximum permissible normal force under dry conditions and to avoid the instability of the friction coefficient at higher relative speeds, the hydraulic jack was used in a second testing series. As it can be seen in Fig. 11, the hydraulic jack is capable of

reaching greater normal forces as well as increasing the stiffness of the tribometer. Consequently, a decrease in friction coefficient with increasing relative speeds can be observed. Only for relative speeds of $v_{rel} = 65$ m/min and $v_{rel} = 89$ m/min an increase of friction coefficient can be seen.

### 3.3. Overarching discussion

All results of the two series of tests on the different tribometers were compiled in a plot, which is shown in Fig. 12. The values of the friction coefficients and average apparent contact pressures as a function of the relative speeds were plotted for both test rigs in dry and lubricated condition. As the pneumatic jack leads to inexplicable results under dry conditions, the results of the hydraulic jack were compared to the friction coefficients of the translational movement. However, the use of the hydraulic jack has to be regarded in more detail due to the intervention conditions. As the hydraulic jack induces a greater stiffness, tribological phenomenon, like the stick-slip effect, could suppress the ongoing processes within the contact zone.

In Fig. 12, it can be seen that the values and the course of the friction coefficient over the relative speed for the dry condition correspond very well between the two test rigs.

The high apparent coefficients of friction, that were already determined by [25] for the material pairing in the dry state at low relative speeds, were confirmed by both experimental setups and can be attributed to the adhesive material behaviour of AISI 316L. The tendency of decreasing friction coefficients with increased cutting speed can be explained by the fact that in both experimental setups, comparable relative speeds and normal forces were applied, leading to similar friction coefficients and, consequently, similar dissipated friction power (1).

$$P = \mu_{app} \times v_{rel} \times F_n \quad (1)$$

For translational movement average normal loads are between $F_n = 400…1000$ N. For rotatory movement the normal loads depend on the used jack and amount $F_n = 100…500$ N. Assuming an identical heat partitioning, it can be stated that the temperature locally reached at the contact point should be very similar. As of now, although this evolution with increasing relative speed is not fully understood, there is a consensus that it might be primarily associated with thermal softening, leading to a decrease of tangential forces. Thereby explaining the similarity of the friction results, especially in dry condition, of both experimental setups.

In the case of the lubricated condition, a different behaviour is found. As expected, the values for the lubricated condition are significantly lower than for the dry condition for both test rigs, and in both cases the dependence on the relative speed is very low. However, the values for the rotating tribometer are systematically significantly lower than those for the translational one. Thus, presumably due to the continuous supply of the fluid in combination with the sparse engagement of the pin, there appears to be a more pronounced lubrication effect. This finding motivates to critically question the transferability of the values for the lubricated contact to the chip formation zone and to further investigate in future studies.

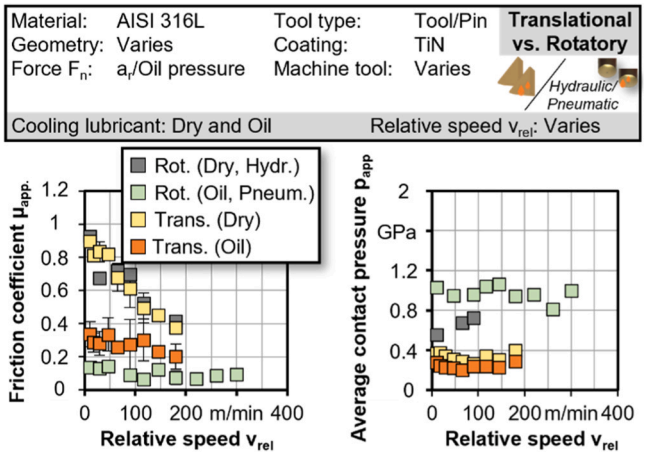


**Fig. 12.** Apparent Friction coefficients and average apparent contact pressures depending on relative speed under dry and lubricated conditions (translational and rotatory relative motion).

In addition to the coefficients of friction, the average apparent contact pressures were determined. The calculation was based on the contact normal forces and the corresponding contact areas. It can be seen that the contact pressures show significant differences depending on the experimental setup. This is partly due to the complexity of determining the actual contact area as well as the different evaluation methods used. The procedures can be taken from [12,15]. By using Pins, the contact diameter was $d \approx 1.2$ mm ($A \approx 1.13$ mm$^2$). Using translational setup, contact area was measured to $A \approx 2.3$ mm$^2$. The high normal force when using the hydraulic jack under dry conditions (see Fig. 11) could not be used to determine all average contact normal pressures on the basis of the current post-processing tool. This is due to instabilities in the simulation used with high normal forces and simultaneously high friction coefficients. Being capable of calculating the average contact normal pressures over the entire test region is part of future studies.

Nevertheless, in both configurations, the contact conditions result in a plastic sliding contact. Consequently, the contact pressure cannot be evaluated using Hertz elastic contact theory. Due to the severity of these conditions, the fully plastic state is rapidly attained, and the mean pressure in the contact area is restricted by the flow stress of the material itself, typically around three times the yield stress as indicated by Johnson [28]. Therefore, once a relatively high normal load is applied, causing plastic deformation of the solids, the limit of contact pressure is commonly reached. For AISI 316L steel, the yield stress at a temperature of $T = 800$ °C, that represents an exemplary temperature within the contact zone, is approximately $k = 0.23$ GPa. Comparing this with the contact pressures (see Fig. 12), it shows that plastic deformation occurred in both experimental setups. Schulze et al. discussed the transferability of tribometer tests to metal cutting process. He demonstrated that employing a tribological setup, inducing plastic deformation at high relative speeds, with or without preheating temperature, leads to relevant contact conditions for investigating friction phenomena in metal cutting. Further increasing the normal load merely leads to an expansion of the contact area [29]. This observation supports the idea that a comparable mean contact pressure is locally achieved in both setups.

## 4. Friction modelling and 2D chip formation simulation

In addition to gaining knowledge about the tribology of the chip formation zone, the experiments on friction characterisation under machining like conditions pursue the purpose of generating a database for friction modelling in numerical chip formation simulations. For this reason, parts of the generated test data in dry condition (translational movement) are used in the following to determine empirical models of the friction coefficient as a function of the relative speed as well as relative speed and temperature and to investigate their influence on a chip formation simulation. Although Challen et al. proposed, that the apparent friction coefficient is calculated by an addition of the macroscopic plastic deformation friction coefficient and the local interfacial adhesive friction coefficient [30], in this study the assumption $\mu_{app} \approx \mu_{adh}$ is made.

### 4.1. Friction modelling depending on relative speed

Fig. 13 shows the basic procedure of friction modelling using the example of TiN-coated tools. First, the experimental measured values

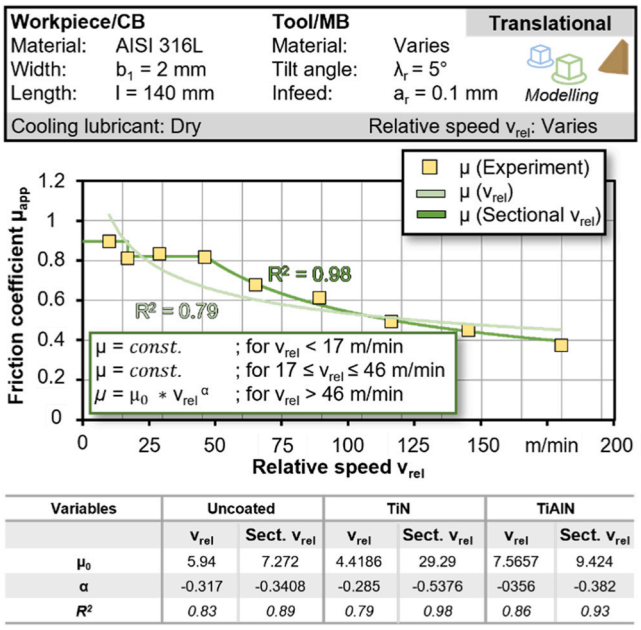


| Variables | Uncoated | | TiN | | TiAlN | |
|---|---|---|---|---|---|---|
| | $v_{rel}$ | Sect. $v_{rel}$ | $v_{rel}$ | Sect. $v_{rel}$ | $v_{rel}$ | Sect. $v_{rel}$ |
| $\mu_0$ | 5.94 | 7.272 | 4.4186 | 29.29 | 7.5657 | 9.424 |
| α | -0.317 | -0.3408 | -0.285 | -0.5376 | -0356 | -0.382 |
| $R^2$ | *0.83* | *0.89* | *0.79* | *0.98* | *0.86* | *0.93* |

**Fig. 13.** Friction modelling for uncoated and coated tools using a relative speed and a sectional relative speed dependent friction model.

are plotted. These can then be described with various functional equations. A common approach for the dependence of the friction coefficient on the relative speed in dry machining is the power function (light green curve). However, since the results of the experiments showed a constant course for low relative speeds, this approach shows a comparatively low coefficient of determination of $R^2 = 0.79$.

Accordingly, a sectionally defined model was developed as a further approach that can separately describe the dependencies changing over the relative speed intervals, see Fig. 13.

This consists of constant sections and a subsequent power function. The number of different constant sections as well as the starting point of power function depends on the respective coating. For TiN coating the power function starts at $v_{rel} = 46$ m/min. The model thus follows the physical logic of the differently pronounced friction mechanisms and achieves a very high coefficient of determination of $R^2 = 0.98$.

### 4.2. Friction modelling depending on relative speed and temperature

In this chapter, in addition to the relative speed, the influence of temperature on the friction coefficient is investigated. Fig. 14 shows that independent of the coating, the temperature increases with increasing relative speeds.

While at a relative speed of $v_{rel} = 29$ m/min the temperature measured for TiN and TiAlN coatings was approx. $T = 420$ °C, at $v_{rel} = 180$ m/min the temperature is already $T = 620$ °C. However, it should be noted that the results represent the temperatures on the CB and were measured at a distance of $l = 0.8$ mm behind the contact zone, which therefore implies that the real friction temperature will be higher. The values can be corrected by appropriate post-processing [31].

To parameterise the friction models, first the influence of temperature on the relative speed was approximated linearly using Eq. (2).

$$T = A \times v_{rel} + B \tag{2}$$

In a second step, the friction models were parameterised according to the procedure of Peng et al. [31] using Eq. (3).

$$\mu = a \times \left(\frac{v_{rel}}{c}\right)^{b} \times \left(\frac{T}{e}\right)^{f} \tag{3}$$

Fig. 14 shows both, an example of the friction model for the TiN coating as well as the variables fitted for uncoated, TiN- and TiAlN-coated tools. The calculation was carried out in *Matlab* by solving a least square nonlinear equation with the Levenberg–Marquardt optimisation method. The coefficient of determination $R^2 > 0.9$ shows that a high approximation quality could be achieved. Assuming that both, the relative speed and the contact pressure influence the temperature, the friction coefficient decreases with increasing temperature, see Fig. 14. This behaviour can be traced back to thermal softening effects, that occur by higher temperatures and reduce the limited shear stress of the AISI 316L. At the same time, internal friction, that can be explained by the assumption of fluid material movement in the contact zone, is increased by rising temperatures, which increases the friction coefficient [32]. Therefore, the real influence of temperature on friction coefficient can only be determined by an isolated consideration of the influencing variables [31].

### 4.3. 2D chip formation simulation

2D chip formation simulations were carried out to validate the developed friction models for translational movement. The computer used had an Intel® Xeon W1390 processor with 6 cores and a maximum clock frequency of 5.3 GHz (64 GB RAM). Only one core was used within the 2D-simulation. The total simulation time amounted approximately $t \approx 10$ h for a cutting path of $l = 5$ mm. For accelerated heating of the tool, the heat transfer coefficient was set to $h = 40{,}000$ W/m$^2$°C. The other key boundary conditions of the simulation model, created in DEFORM 2D version 13.1, are shown in Table 2, Table 3 and Fig. 15.

In a first step, the geometry of the tool respectively the angles were modelled according to the experimental tools. The dimensions of the tool and the workpiece were chosen in such a way that, on the one hand, a steady state is achieved with respect to the mechanical tool loads and, on the other hand, the natural contact length between the chip and the rake face can be formed. In order to realise a high prediction quality with acceptable computation time, a graded meshing was introduced at the workpiece as well as at the tool, so that a higher information density could be realised in areas of high gradients of the state variables. For the yield stress, the Johnson-Cook model was used, with three different

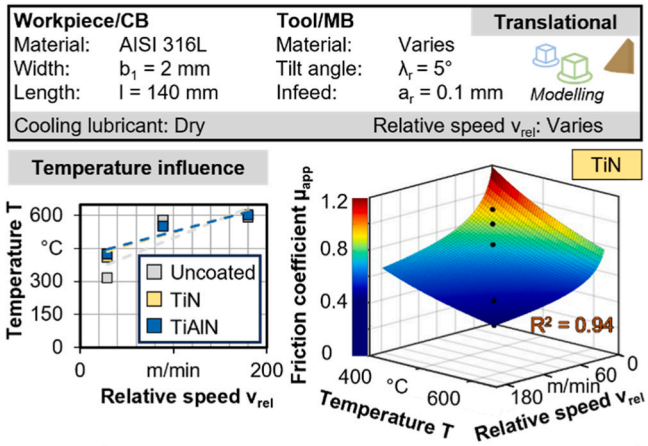


| | Variables | Uncoated | TiN | TiAlN |
|---|---|---|---|---|
| Temperature (Linear Eq.) | A | 0.1017 | 0.0736 | 0.0676 |
| | B | 328.67 | 400.18 | 414.15 |
| | $R^2$ | *0.68* | *0.86* | *0.88* |
| Friction model f($v_{rel}$; temperature) | a | 1.287 | 2.651 | 3.613 |
| | b | -0.1254 | -0.1973 | -0.2536 |
| | c | 1.435 | 629.9 | 209.9 |
| | e | 553.1 | 140.6 | 138.1 |
| | f | -0.9997 | -1 | -1 |
| | $R^2$ | *0.94* | *0.94* | *0.98* |

**Fig. 14.** Friction modelling for TiN coated tools using a sectional relative speed and temperature dependent friction model.

**Table 2**
Properties of stainless steel AISI 316L.

| | AISI 316L |
|---|---|
| Young modulus (MPa) | Temp. dep. (DEFORM) |
| Poisson coefficient | 0.3 |
| Density (g/cm$^3$) | $8.0 \times 10^{-9}$ |
| Reference temperature (°C) | 20 |
| Thermal expansion | Temp. dep. (DEFORM) |
| Thermal conductivity (W/m °C) | Temp. dep. (DEFORM) |
| Heat capacity (J/K) | Temp. dep. (DEFORM) |
| Emissivity | 0.7 |

**Table 3**
Properties of uncoated and coated cemented carbide.

| *D = DEFORM | Uncoated | TiN | TiAlN |
|---|---|---|---|
| **Young modulus (MPa)** | 650,000 | 600,000 | 440,000 |
| **Poisson coefficient** | 0.25 | 0.25 | 0.23 |
| **Density (g/cm$^3$)** | $8.0 \times 10^{-9}$ | $5.22 \times 10^{-09}$ | $5.22 \times 10^{-09}$ |
| **Reference temperature (°C)** | 20 | 20 | 20 |
| **Thermal expansion** | $5 \times 10^{-06}$ | $9.4 \times 10^{-06}$ | $9.2 \times 10^{-06}$ |
| **Thermal conductivity (W/m °C)** | Temp. dep. (*D) | 25 | Temp. dep. (*D) |
| **Heat capacity (J/K)** | 4.68 | 3.24 | 2.88 |
| **Emissivity** | 0.5 | 0.3 | 0.5 |

parameter sets, also shown in Fig. 15.

These parameter sets based on the one hand, on own Split-Hopkinson-Pressure-Bar (SHPB) experiments and on the other hand on an established parameter set from the literature, as well as a combination of the two.

Finally, the simulation results were validated using experimental measured data of an orthogonal cut. The results of this validation are shown in Fig. 16, where both the cutting force and the feed force are plotted. However, the feed force acts as the central validation variable for the friction model.

In a first step, a flow stress model with a good prediction quality of feed- and cutting force ($\Delta F_f = -3.2\%$; $\Delta F_c = +16.7\%$) was selected. In this step the relative dependent friction model was modelled using power function, see Fig. 13.

Subsequently, the power function model, the sectional model and the sectional and temperature dependent model of the friction coefficient were compared using the flow stress model from Tounsi et al. + SHPB. The sectional model was able to provide a very good prediction of the passive force with a percentage deviation of $\Delta F_f = +0.9\%$, whereas cutting force deviation was slightly increased to $\Delta F_c = +18.4\%$ compared to the relative speed dependent model. The friction model, considering both relative speed and temperature, significantly underestimates the feed force ($\Delta F_f = -33.6\%$). However, it can be seen that the cutting force prediction could be improved significantly. The percentage deviation amounts $\Delta F_c = +3.3\%$.

In the third step, a variation of the coating was carried out using the sectional relative speed dependent (step.3.1) as wells as the sectional relative speed and temperature dependent friction model (step.3.2), shown in Fig. 16. It can be seen that the cutting force is consistently overestimated ($\Delta F_c \approx +11\ldots30\%$), whereas the feed forces are slightly underestimated ($\Delta F_f \approx -1\ldots12\%$). Nevertheless, cutting force prediction increases with increasing cutting speed. The increase in cutting speed undoubtedly leads to more intense thermal softening, which is also evident in the main cutting force that decrease with higher cutting speeds. However, the larger deviation with the TiN and TiAlN coating, especially for a cutting speed of $v_c = 175$ m/min, may indicate that certain aspects, such as tribo-chemical reactions, were not fully considered in the proposed friction model for this coating.

Fig. 16 also compares the simulated temperature field on the rake face with experimentally determined rake face temperatures. The procedure for determining the temperatures is based on an extended version of the experimental setup for determining the rake face temperatures in the translational cutting by Saelzer et al. [33]. It should be noted that in all simulations, there is no steady state of the temperatures in the entire contact area ($l_{ch} \approx 0.2$), corresponding to the used measurement diameter, after a cutting path of $l = 5$ mm. The highest prediction quality ($\Delta T_{RF} \approx +/- 5\%$) could be realised with uncoated tools. Independent of the coating, the prediction quality is increased by an increase of the cutting speed.

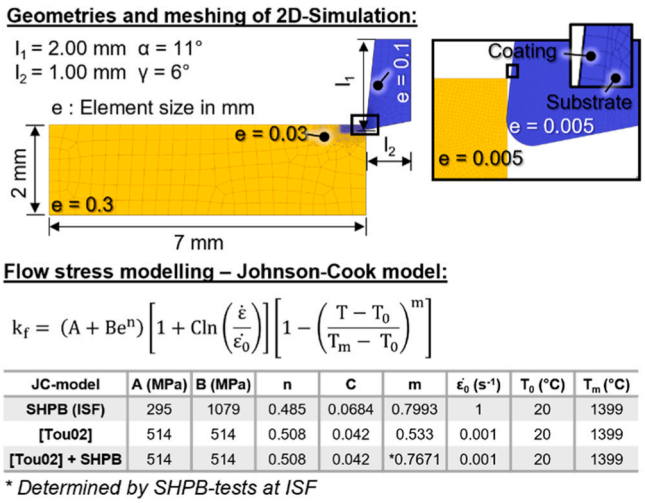


| JC-model | A (MPa) | B (MPa) | n | C | m | $\dot{\varepsilon}_0$ (s$^{-1}$) | $T_0$ (°C) | $T_m$ (°C) |
|---|---|---|---|---|---|---|---|---|
| SHPB (ISF) | 295 | 1079 | 0.485 | 0.0684 | 0.7993 | 1 | 20 | 1399 |
| [Tou02] | 514 | 514 | 0.508 | 0.042 | 0.533 | 0.001 | 20 | 1399 |
| [Tou02] + SHPB | 514 | 514 | 0.508 | 0.042 | *0.7671 | 0.001 | 20 | 1399 |

* Determined by SHPB-tests at ISF

**Fig. 15.** Setup of the chip formation model and material constants for the constitutive equation for AISI 316L.

Finally, in step 3.2, a variation of the coating was carried out using the sectional relative speed and temperature dependent friction model. In Fig. 17 it can be seen that the more accurate prediction of the cutting force also enables a more precise prediction of the temperature field within the contact area on the rake face. The mean deviation from experimentally determined rake face temperatures for uncoated, TiN- and TiAlN-coated tools is $\Delta T_{RF} = +2.5\%$ across both cutting speeds. In the sectional friction model, on the other hand, the temperatures are already overestimated by $\Delta T_{RF} = +10.1\%$, therefore it can be assumed that the temperature dependent friction model will predict more accurate with longer cutting paths up to a steady state in temperature.

To achieve a steady state temperature more quickly, the heat capacity was exemplarily reduced by a factor of 36. This procedure has already been carried out by Childs et al. and serves to achieve a steady state with reasonable calculation times [34]. In this case, heat capacity was $c_p = 0.13$ J/gK for the substrate and 0.08 J/gK for TiAlN coating. As a result of this procedure, a thermal steady state was achieved after $l = 3$ mm cutting path. The temperature deviation amounts to $\Delta T_{RF} \approx +14.2\%$, corresponding to an increase of + 8.8% compared to the evaluated temperature with conventional heat capacity without having thermal steady state. However, it should be mentioned that, depending on the friction model and the coating, the feed force is greatly underestimated with this procedure.

The average simulated interface contact pressure was, in dependence of rake fake position, between $p \approx 1\ldots2$ GPa for all parameter combinations. Thus, it can be traced back that the locally achieved contact pressures in the friction experiments adequately reflect the conditions in the chip formation zone.

In the further course of the project, the parameterised chip formation simulations will provide the basis for further development of wear rate models for uncoated, TiN and TiAlN-coated carbide tools for dry machining of austenitic steel AISI 316L.

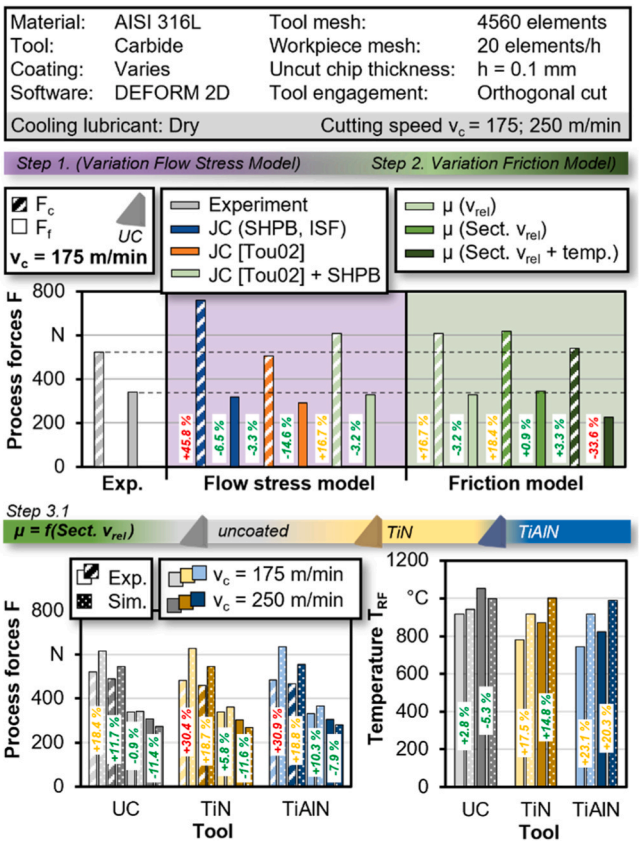


**Fig. 16.** Results of the finite element chip formation simulation: Step 1: Variation of the flow stress model; Step 2: Variation of the friction model; Step 3.1: Variation of the coating using the sectional relative speed dependent friction model.

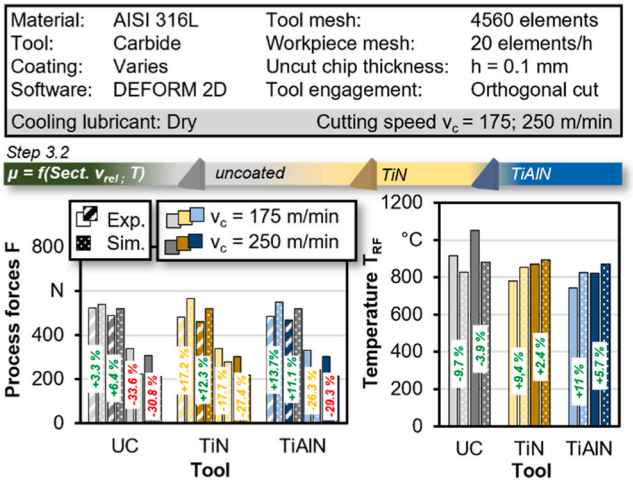


**Fig. 17.** Results of the finite element chip formation simulation: Step 3.2: Variation of the coating using the sectional relative speed & temperature dependent friction model.

## 5. Conclusion and outlook

In the present work, investigations were carried out to characterise friction under machining-like conditions on two different test rigs: a test with translational relative motion with flat contact surface and a pin-on-bar test. It was shown that in the dry state there is good agreement between the measurement results of the friction coefficient. This represents a good mutual validation of the test principles.

For the lubricated case, however, greater differences are found here, the friction coefficient in the case of the pin-on-bar test is at a significantly lower level than in the case of the other tribometer. In addition, three different states of lubrication could be identified in the individual measurement records of the translational tribometer: a strong reduction at the beginning, a transition range with a continuous increase and a semi-lubricated range between the lubricated and the dry. It is concluded that there is a different temporal distribution of lubrication mechanisms over time. Based on the totality of the results, it is suggested that the strong lubrication is primarily a hydrodynamic lubricating film that is thermally discharged during the transition region and that the remaining lubricating effect can be attributed to the tribo-chemical reaction products formed during this process. Finally, an exemplary modelling study was conducted that compared the influence of a relative speed, sectionally relative speed as well as a sectionally relative speed and temperature dependent friction model. It was found that the sectional friction model achieved the highest feed force prediction. The temperature dependent model, on the other hand, underestimated the feed force significantly, whilst providing the highest prediction of the cutting force and rake face temperature.

Future work should further investigate the lubrication mechanisms and their effect on friction. In addition, it must be determined which form of lubrication can be transferred to the chip formation zone and under which conditions. On this basis, the friction modelling for numerical chip formation simulations could then also be advanced.

## Declaration of Competing Interest

The authors declare that they have no known competing financial interests or personal relationships that could have appeared to influence the work reported in this paper.

## Acknowledgements

Funded by the Deutsche Forschungsgemeinschaft (DFG, German Research Foundation) – project number 468249651.

## References

[1] Vakis AI, Yastrebov VA, Scheibert J, Nicola L, Dini D, Minfray C, et al. Modeling and simulation in tribology across scales: an overview. Tribol Int 2018;125:169–99.
[2] Denkena B, Krödel A, Beblein S. A novel approach to determine the velocity dependency of the friction behavior during machining by means of digital particle image velocimetry (DPIV). CIRP J Manuf Sci Technol 2021;32:81–90.
[3] Grzesik W, Rech J. Methods and devices for measuring metal cutting friction and wear. J Mach Eng 2019;19(1):62–70.
[4] Melkote SN, Grzesik W, Outeiro J, Rech J, Schulze V, Attia H, et al. Advances in material and friction data for modelling of metal machining. CIRP Ann 2017;66(2):731–54.
[5] Ozlu E, Budak E, Molinari A. Analytical and experimental investigation of rake contact and friction behavior in metal cutting. Int J Mach Tools Manuf 2009;49(11):865–75.
[6] Sterle L, Pušavec F, Kalin M. Determination of friction coefficient in cutting processes: comparison between open and closed tribometers. Procedia CIRP 2019;82:101–6.
[7] Olsson M, Soderberg S, Jacobson S, Hogmark S. Simulation of cutting tool wear by a modified pin-on-disc test. Int J Mach Tools Manuf 1989;29(3):377–90.
[8] Smolenicki D, Boos J, Kuster F, Roelofs H, Wyen CF. In-process measurement of friction coefficient in orthogonal cutting. CIRP Ann 2014;63(1):97–100.
[9] Zemzemi F, Bensalem W, Rech J, Dogui A, Kapsa P. New tribometer designed for the characterisation of the friction properties at the tool/chip/workpiece interfaces in machining. Tribotest 2008;14(1):11–25.
[10] Puls H, Klocke F, Lung D. A new experimental methodology to analyse the friction behaviour at the tool-chip interface in metal cutting. Prod Eng Res Dev 2012;6(4-5):349–54.
[11] Hedenquist P, Olsson M. Sliding wear testing of coated cutting tool materials. Tribol Int 1991;(23, 3):143–50.
[12] Mondelin A, Claudin C, Rech J, Dumont F. Effects of lubrication mode on friction and heat partition coefficients at the tool–work material interface in machining. Tribol Trans 2011;54(2):247–55.

[13] Cabanettes F, Rolland J, Dumont F, Rech J, Dimkovski Z. Influence of minimum quantity lubrication on friction characterizing tool–aluminum alloy contact. J Tribol 2016;138(2).
[14] Puls H, Klocke F, Lung D. Experimental investigation on friction under metal cutting conditions. Wear 2014;310(1-2):63–71.
[15] Nobel C, Hofmann U, Klocke F, Veselovac D, Puls H. Application of a new, severe-condition friction test method to understand the machining characteristics of Cu–Zn alloys using coated cutting tools. Wear 2015;344-345:58–68.
[16] Saelzer J, Berger S, Iovkov I, Zabel A, Biermann D. Modelling of the friction in the chip formation zone depending on the rake face topography. Wear 2021;477:203802.
[17] Saelzer J, Alammari Y, Zabel A, Biermann D, Lee J, Elgeti S. Characterisation and modelling of friction depending on the tool topography and the intermediate medium. Procedia CIRP 2021;102:435–40.
[18] Rech J, Kusiak A, Battaglia J. Tribological and thermal functions of cutting tool coatings. Surf Coat Technol 2004;186(3):364–71.
[19] Volke, P., Brock, G., Berger, S., Saelzer, J., Nickel, J., Biermann, D. Sustainable production of rotationally symmetrical components: Approaches to resource saving on tool and workpiece. In: Proceedings of the ASME 2022 - International Mechanical Engineering Congress and Exposition IMECE2022 2022.
[20] Segebade E, Schneider J, Schulze V. Tribological effects in and by metal cutting. KEM 2018;767:3–24.
[21] Banerjee N, Sharma A. Identification of a friction model for minimum quantity lubrication machining. J Clean Prod 2014;83:437–43.
[22] Machado Alisson R, da Silva Leonardo RR, de Souza Felipe CR, Davis Rahul, Pereira Leandro C, Sales Wisley F, et al. State of the art of tool texturing in machining. J Mater Process Technol 2021;293:117096.
[23] Bierla A, Fromentin G, Minfray C, Martin J-M, Le Mogne T, Genet N. Mechanical and physico-chemical study of sulfur additives effect in milling of high strength steel. Wear 2012;286-287:116–23.
[24] Minfray C, Fromentin G, Bierla A, Martin J-M, Le Mogne T. The effect of an organic pentasulfide EP additive in turning and milling operations. Wear 2014;317(1-2):129–40.
[25] Valiorgue F, Rech J, Hamdi H, Bonnet C, Gilles P, Bergheau JM. Modelling of friction phenomena in material removal processes. J Mater Process Technol 2008;201(1-3):450–3.
[26] Bonnet C, Valiorgue F, Rech J, Claudin C, Hamdi H, Bergheau JM, et al. Identification of a friction model — application to the context of dry cutting of an AISI 316L austenitic stainless steel with a TiN coated carbide tool. Int J Mach Tools Manuf 2008;48(11):1211–23.
[27] Behera BC, Chetan, Ghosh S, Rao PV. The underlying mechanisms of coolant contribution in the machining process. In: Machining and Tribology. Elsevier; 2022. p. 37–66.
[28] Johnson KL. Contact Mechanics. London: Cambridge University Press,; 1985.
[29] Schulze V, Bleicher F, Courbon C, Gerstenmeyer M, Meier L, Philipp J, et al. Determination of constitutive friction laws appropriate for simulation of cutting processes. CIRP J Manuf Sci Technol 2022;38:139–58.
[30] Challen JM, Oxley PLB. An explanation of the different regimes of friction and wear using asperity deformation models. Wear 1979;53:229–43.
[31] Peng B, Bergs T, Schraknepper D, Smigielski T, Klocke F. Development and validation of a new friction model for cutting processes. Int J Adv Manuf Technol 2020;107(11-12):4357–69.
[32] Bobzin K, Brögelmann T, Kruppe NC, Hoffmann DC, Klocke F, Mattfeld P, et al. Tribological studies on self-lubricating (Cr,Al)N+Mo:S coatings at elevated temperature. Surf Coat Technol 2018;353:282–91.
[33] Saelzer J, Berger S, Iovkov I, Zabel A, Biermann D. In-situ measurement of rake face temperatures in orthogonal cutting. CIRP Ann 2020;69(1):61–4.
[34] Childs TH, Arrazola P-J, Aristimuno P, Garay A, Sacristan I. Ti6Al4V metal cutting chip formation experiments and modelling over a wide range of cutting speeds. J Mater Process Technol 2018;255:898–913.